



Simultaneous Investigation of Flexibility and Plasma Actuation Effects on the Aerodynamic Characteristics of an Oscillating Airfoil

A. Mahboubi Doust, A. Ramiar and M. Dardel

Department of Mechanical Engineering, Babol Noshirvani University of Technology, Babol, Mazandaran, 71167-47148, Iran

†Corresponding Author Email: aramiar@nit.ac.ir

(Received May 6, 2015; accepted November 2, 2015)

ABSTRACT

In this work, a numerical study of two dimensional laminar incompressible flow around the flexible oscillating NACA0012 airfoil is performed using the open source code OpenFOAM. Oscillatory motion types including pitching and flapping is considered. Reynolds number for these motions is assumed fixed at 12000. One of the important issues that must be considered in designing air structures, in particular the aircraft wing, is the interaction between the air and the elastic aircraft wings that is known as the Aeroelastic phenomenon. For this purpose, the effect of airfoil flexibility and flow induced vibration in these motion types is investigated and compared with the case of rigid airfoil. It is observed that the flexibility in both types of motions causes improvement of the thrust which is boosted with increasing the frequency. Contrary to thrust, the significant improvement of lift is only achievable in high frequencies. It was also found that the effect of flexibility on the flapping motion is higher than the pitching motion. For flow control on the airfoil, Dielectric Barrier Discharge plasma actuator is used in the trailing edge of a flexible airfoil, and its effect on the flexible airfoil is also investigated.

Keywords: Airfoil; Flapping; Flexibility; Fluid-structure interaction; Oscillating; Plasma; Pitching.

NOMENCLATURE

A	pitching amplitude	\mathbf{v}	velocity of the continuum
\mathbf{b}	body force	\mathbf{v}_s	velocity of surface
c	airfoil chord length	\mathbf{v}	particle velocity
C_L	lift coefficient	\mathbf{v}^m	grid point velocity
C_T	thrust coefficient	ρ	mass density
E	electric field strength	ρ_e	electron number density
e_e	charge of the electron	ρ_s	continuum density
h	plunging amplitude	$\boldsymbol{\sigma}$	cauchy stress tensor
k	reduced frequency	γ	diffusion coefficient
\mathbf{n}	unit normal	\mathcal{G}	frequency of the applied voltage
\mathbf{S}	strain rate tensor	μ	dynamic viscosity
U_a	applied voltage		

1. INTRODUCTION

1.1 Fluid-Structure Interaction (FSI)

Many engineering systems more or less deal with the interaction between the fluid flow and solid

structures. The number of applications that include FSI effects is nearly limitless. Typical examples include: Vibration of bridges and tall buildings due to wind, Aeroelastic deformation of airfoils and rotor blades, and physiological expansion and contraction of blood vessels.

Campbell (2010) stated that the fluid-structure interaction is the interaction of dynamic or deformable structure immersed in a fluid and or contains a fluid. Solid motion alters the stress acting on the solid wetted surface, which in turn causes a change in the motion of the solid. The model that contains such an interaction should be two-way coupling, where the fluid motion affects solid motion and vice versa. In addition, FSI may contain oscillatory or non-oscillatory interactions. Oscillatory interaction occurs when the solid deforms toward its original configuration under strain due to the fluid forces to reduce the strain, but is forced back into the strained configuration once again by the fluid forces. This interaction is continually going on, and gives a solid oscillatory motion. Non-oscillatory interactions are those that cause a steady or quasi-steady strain in the solid due to fluid forces.

Historically, due to insufficient computational resources, the fluid-structure interaction was either ignored or simplified as a one-way coupling. A typical one-way coupling includes tractions imposed on the solid structure based on calculated load of fluid flow. This allows engineers to construct a strong structure to deformation in the allowed range for different fluid flow conditions. One-way coupling does not take into account the effect of solid deformation to flow field, and that's what its importance increases when the deformation is larger. Although this has been acceptable in the past, the present trend for designing of lighter and more efficient structures, especially in the aerospace industry, shows that the FSI effects in the design of engineering systems will be considered in the future.

Many researchers studied the oscillating airfoils, but did not consider the fluid-structure interaction. For example, recently, Kim and Chang (2014) experimentally investigated the effect of low Reynolds number flow in the range of $2 \times 10^4 \leq Re \leq 5 \times 10^4$ on the aerodynamic characteristics of a pitching NACA0012 airfoil, with sinusoidal motion equation of $\alpha_0 + \alpha_1 \sin(\omega t)$. The tests were performed for mean angle of attack (α_0), oscillation amplitude (α_1) and constant reduced frequency (k) of 0, 6 and 0.1, respectively.

But, Tang *et al.* (2008) presented a method of fluid-structure coupling between Navier-Stokes solver and three dimensional FEM beam solver with highlighting some of the aerodynamic concepts. They presented a model about the NACA0012 wing with aspect ratio of 3 in the pure plunging motion and compared their results with the available experimental data. Comparison was performed with test for the rigid wing and the effects of wing flexibility on aerodynamic introduced qualitatively. They observed that the phase lag of the wing tip displacement relative to flapping motion becomes more visible as the fluid density increases.

Unger *et al.* (2008) employed a multiphysical method for numerical analysis of a flexible and

oscillating jig-shape airfoil, in order to investigate the aeroelastic effects. Further, they presented the analysis of low-Reynolds-number flows past this flexible and flapping airfoil where transition from laminar to turbulent flow takes place along a laminar separation bubble. To predict the transition point, they fully coupled a linear stability solver to an URANS flow analysis code. They introduced a partitioned coupling procedure, which used a load and energy conservative data transfer scheme and a qualitative grid deformation based on finite elements. They explained that using a transition prediction method together with the grid deformation has led to the need of an automatic adjustment of the transition location for the updated grid.

Olivier *et al.* (2009) simulated plunging motion of flexible plate by using the open source code, OpenFOAM. They first investigated the effects of flexibility related to flight of Nano Air Vehicles in terms of FSI. The calculated average drag coefficient for the flexible case was about half of the drag coefficient for rigid case, but the average lift coefficient did not change. It is also observed that with small density ratio of solid to fluid or small time steps solutions were unsteady. In fact, the problem may lie in the weakness of the code written by them which was usable just for a simple geometry and weak coupling.

Unger *et al.* (2012) used a coupled simulation method to evaluate the fluid flow around a lightweight and flexible airfoil according a seagull handfoil. Finite element model of the flexible airfoil was fully coupled to the flow solver by using a load and displacement transfer as well as a fluid grid deformation algorithm. Flow field was specified by a laminar-turbulent transition at a Reynolds number of $Re=100000$, in which a laminar separation bubble occurs. An unsteady Reynolds-averaged Navier-Stokes flow solver was used. Their results showed that flexible airfoil has a major impact on the efficiency of thrust, mean lift and drag, and the location of laminar-turbulent transition. Thrust efficiency can be improved considerably by the plunging amplitude and using time-dependent airfoil stiffness, inspired by muscle contraction of birds.

Lee and Lee (2012) presented a computational fluid-structure interaction analysis, especially for flexible structures. A flexible plate was placed normal to a free stream and flow around it, was simulated to investigate the effects of flexibility on the flow. The lattice Boltzmann method with an immersed boundary technique using a direct forcing scheme was used to simulate the fluid, and a finite element method with Euler beam elements was used to model the flexible plate. Their results showed that the flexibility of the plate significantly influences the reduction of the force coefficients induced by the flow.

Ducoin *et al.* (2012) conducted some tests on a flexible hydrofoil in static and transient regimes with measurement techniques based on image processing and Laser Vibrometry, for non cavitating

and cavitating flows. For the non cavitating flow, they observed that for small values of pitching velocity, a displacement inflection occurs due to the laminar to turbulent transition whereas the highest pitching velocity suppresses the effect. Also low frequency fluctuating displacements have been observed when leading edge vortex shedding occurs during the stall. For the cavitating flow, they measured the vibration of the structure for a fixed angle of attack and showed that cavitation highly excite the natural frequencies of the hydrofoil, in particular for pulsating cavities.

Lapointe and Dumas (2012) studied self-sustained pitch-heave oscillation phenomenon at transitional Reynolds numbers by using two dimensional URANS Spalart-Allmaras and γ - Re_θ models. They compared predicted pitching and heaving amplitudes and frequencies of the oscillations with previous experimental results. They considered an elastically-mounted rigid body with two-degrees-of-freedom, pitch and heave, thus in their paper the effect of airfoil flexibility is not considered. The purpose of their paper is to demonstrate the ability of modern CFD to capture and reproduce the observed complex coupling between the flow and the elastic structure.

Veilleux and Dumas (2013) compared two-dimensional numerical simulation of fluid-solid model using Spalart-Allmaras turbulence model with the experimental results. They also carried out laminar and $k\omega$ -SST simulations. The airfoil was elastically mounted on a linear spring-damper base in heave and a rotational spring-damper base in pitch motion. The airfoil is free to pitch and heave independently; no mechanical linking is enforced between both degrees of freedom. The results obtained by laminar calculations were relatively in good agreement with the experimental data for both structural heave stiffnesses investigated. Results obtained by the turbulence models agreed well with the experiments for the cases where the airfoil's dynamics is dominated by the structural stiffness, and did not match so good with the experiments for the cases where the aerodynamic plays a more significant role on the airfoil's dynamics.

Lee and Lee (2013) numerically analyzed the fluid-structure interaction for a flapping flexible plate moved with propulsive velocity in a quiescent fluid to investigate the effect of flexibility on propulsive velocity, which is critical for fish, birds, insects, and micro air vehicles with flapping wings. The method used in this paper was similar to their previous paper. Their study lead two main results, first the mechanism of the flapping plate, moved with propulsive velocity, differs from that of the plate fixed in propulsive direction. For the faster cruised velocity, the rigid plate with symmetrical rotation was more efficient than the plate with advanced rotation, even with less propulsion force. Second, they found that the flexibility of the plate improves the propulsive velocity to create an optimal point in the propulsion, which produces twice the velocity as the rigid plate.

1.2 Flow Control Based on Plasma Actuator

Flow control is defined as manipulation of flow field to create a favorable change. Flow passing through the outer surface of a body such as an aircraft or submarine can be manipulated for the following purposes:

1. Delaying the transition
2. Delaying the separation
3. Increasing the lift
4. Decreasing the pressure drag and skin friction.

There are several categories for flow control. The method used in this paper is a type of active method called ElectroHydroDynamic (or EHD), that increases the lift and reduces the drag in the majority of cases. Since the beginning of the 50s onwards, this method has been a topic of serious discussion in the mechanics of the aerospace industry and scientific research. Creating a driving force for a submarine or ship, creating thrust in the supersonic and ultrasonic flow, flow shock control in the inlet jet, control of complex phenomena in fluid flow near the wall such as boundary layer, turbulence, vortex flow and separation are among the applications of this field of science.

Flow control over airfoils has great importance in the design of air vehicles. There are several actuators to control the flow but recently Dielectric Barrier Discharge (DBD) plasma actuators have attracted attention of researchers e.g. Corke *et al.* (2007) as an aerodynamic flow control device. This actuator usually consists of an exposed electrode and an embedded electrode, separated by a dielectric sheet. The electrodes are energized at high voltages and frequencies, causing the air over the embedded electrode to ionize, and finally produce a micro jet near the surface. The typical asymmetric electrodes configuration of the single dielectric-barrier discharge (SDBD) is shown in Fig. (1) by Zhang *et al.* (2009). Since the plasma actuator is fully electronic and does not need moving components, it has quick response and light weight, also it needs low input power.

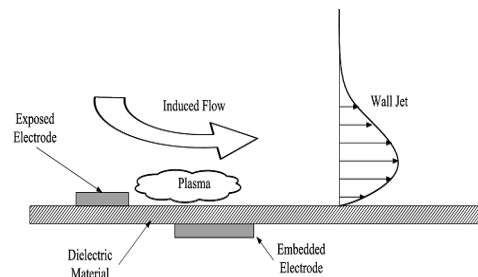


Fig. 1. Asymmetric electrodes configuration of the single dielectric-barrier discharge (SDBD).

Abdollahzadeh *et al.* (2012) investigated the effect of Dielectric Barrier Discharge (DBDs) actuator to improve the flow characteristics over a NACA 0021 airfoil at 23 deg angle of attack and velocity of 35 m/s. They considered the plasma as a body force

added to the momentum equation. The results showed that the plasma actuator can induce an acceleration to the flow close to the surface and thus cause a decrease in the size of separation bubble.

Mukherjee and Roy (2012) used large eddy simulation to model the two-dimensional flow passing over an oscillating NACA0012 airfoil at $Re = 1.35 \times 10^5$ and theoretically predicted the effect of plasma actuator as a flow control device on such an oscillating airfoil. Results were provided for plasma actuators located at the leading edge, mid-chord and trailing edges in both co-flow and counter flow configurations. Results showed that depending on the location of the actuator, up to 29.2% more lift and 12.5% less drag can be obtained. Such improvements in the lift and drag characteristics through the use of plasma actuation indicate a very useful application of such flow control devices in enhancing the performance of oscillating airfoils.

Walker and Segawa (2012), used the dielectric barrier discharge plasma actuators for active control of flow separation over a NACA0024 airfoil. Experiments were conducted at a free stream velocity up to $U \approx 10 \text{ m/s}$ ($Re = 1.3 \times 10^5$) in an open-circuit blower type wind tunnel with a test section of dimensions $200\text{mm} \times 200\text{mm} \times 600\text{mm}$. Performance comparisons were made between electrodes located at the leading edge (LE) and the quarter chord (QC, 25% of chord length) at angles of attack $\alpha = 8^\circ, 12^\circ, 16^\circ$. They concluded that the active flow control by DBD plasma actuator is successful at low Reynolds numbers, but at high Reynolds numbers power consumption increases, because a separation bubble with much larger momentum grows from the trailing edge. In that case, tangential jets injected toward the free stream direction will not be effective, but longitudinal vortex for sucking separated flow in the direction of wing surface seems to be promising.

In this work, a numerical study of two dimensional laminar incompressible flow around a flexible oscillating NACA0012 airfoil is performed using the OpenFOAM. Oscillatory motion types including pitching and flapping is considered. Reynolds number for these motions is assumed fixed at the value of 12000. The effect of these motions and also unsteady parameters such as reduced frequency on the aerodynamic coefficients is investigated. In addition, a numerical FSI code in OpenFOAM that is capable of solving the strong coupling and strong impact of high oscillation frequencies on the geometry is developed and validated with Hron and Turek (2006) benchmark. Then, the effect of airfoil flexibility and flow induced vibrations on the airfoil, as well as the plasma flow control and reduced frequency on the aerodynamic coefficients are investigated and compared with the rigid airfoil. With an overview of previous works, to the knowledge of the authors, the simultaneous effect of oscillating motion, plasma and flexibility of the airfoil has not been studied yet. Moreover, the previous FSI solvers were restricted to limited

density ratios and deformation and a simple geometry as well. Thus, this paper is a step forward compared to the previous works, by employing a more rigorous solver. This paper is extracted from the results of a main project, the core objective of which is investigation of the flutter stability at high frequencies and amplitudes, and will be presented in future works.

2. GOVERNING EQUATIONS

The vast majority of studies used FSI solvers that utilize Arbitrary Lagrangian-Eulerian formulation (ALE) for flow solver. This formula changes the fluid mesh form in response to deformation of the solid. Alternatives of ALE, including immersed boundary, the fictitious domain, and the mortar finite element method, are partly included Lagrangian coefficient method and use the fixed fluid grids. Tezduyar *et al.* (2008) described advantages of ALE over the fixed-mesh approaches; ALE has the ability to maintain a high quality mesh near the surface of the solid interface, and thus leads to more accurate solutions in the area of fluid mechanics. For geometries with a high complexity, often in addition to the mesh motion, mesh refinement is also required. Accordingly, the ALE method is used in this paper.

The governing equations for both the fluid and solid domains differ only in their structural relationships and in this section, first the resulting overall equation for continuum mechanics and then characteristics of each domain are presented. Equations in ALE provide a very general framework that takes Euler, Lagrange, or an arbitrary viewpoints. The first equation is the continuity equation that is shown by Campbell (2010):

$$\frac{\partial \rho}{\partial t} + \nabla \cdot [\rho(\mathbf{v} - \mathbf{v}^m)] = 0 \quad (1)$$

Where ρ is the mass density, \mathbf{v} is particle velocity (liquid or solid), and \mathbf{v}^m is grid point velocity. To apply the Lagrangian approach, $\mathbf{v} = \mathbf{v}^m$ and for Eulerian, $\mathbf{v}^m = 0$. Performing a force balance and using the continuity equation leads to the following momentum equation:

$$\rho \frac{\partial \mathbf{v}}{\partial t} + \rho [(\mathbf{v} - \mathbf{v}^m) \cdot \nabla] \mathbf{v} = \nabla \cdot \boldsymbol{\sigma} + \rho \mathbf{b} \quad (2)$$

Where $\boldsymbol{\sigma}$ is the Cauchy stress tensor and \mathbf{b} is the body force due to plasma.

Kamakoti and Shyy (2004) stated that a necessary condition for the ALE is that mesh velocity must satisfy the geometric conservation law:

$$\rho \frac{\partial V^{ce}}{\partial t} + \nabla \cdot \mathbf{v}^m = 0 \quad (3)$$

Where V^{ce} is the volume of a control element. GCL states that change of volume of each control volume

between the two adjacent time steps is equal to the volume swept by the cell boundary during the time step.

Two predominant methods for solving are the finite element method (FEM) and the finite volume method (FVM). Both of the solid and flow solvers in this paper use the FVM. In the FVM, the computational domain is divided into a set of discrete volumes δV_i that fill the computational domain, D , without overlap. Then the fluid flow equations are integrated over each individual finite volume δV_i . Gauss divergence theorem is used to convert the terms in Eqs. (1) and (2) into terms of surface integral flux, the problem is simplified with discretizing these terms to find difference flux approximations based on central values of certain cells.

2.1 Flow Solver

For Newtonian fluids under incompressible flow condition the following approximation is used for the stress tensor:

$$\sigma = -p\mathbf{I} + 2\mu\mathbf{S} \quad (4)$$

Where p is the thermodynamic pressure, μ is absolute viscosity and \mathbf{S} is the strain rate tensor. Replacing Eq. (4) in the momentum equation (Eq. (2)) and using $2\nabla \cdot \mathbf{S} = \nabla^2 \mathbf{v}$, the Navier-Stokes equation becomes:

$$\frac{\partial \mathbf{v}}{\partial t} + \left[(\mathbf{v} - \mathbf{v}^m) \cdot \nabla \right] \mathbf{v} = -\frac{1}{\rho} \nabla p + \nu \nabla^2 \mathbf{v} + \mathbf{b} \quad (5)$$

Plasma is produced by adding sufficient amount of energy to a molecular gas. This energy can be transferred to electrons and ions, by applying a voltage to electrodes through the electric field. At high frequencies, the charged particles will arrive to high speeds. Although the electrons are faster than ions, but due to their small mass, their direct impact on the momentum transfer is very small. So the momentum transfer between plasma and its ambient will be carried out via ions. Electrostatic pressure due to the electric field pushes the fluid away. To calculate the body force applied by plasma, formulation of Shyy *et al.* (2002) is used. As the field strength decreases with distance from the source, it can be stated as follows:

$$|E| = E_0 - k_1 x - k_2 y \quad (6)$$

Where E_0 can be approximated as follows:

$$E_0 = \frac{U_a}{d} \quad (7)$$

Finally components of body force due to plasma which must be entered in the momentum equation are:

$$b_x = g\alpha\rho_c e_c \Delta t E_x \delta, \quad b_y = g\alpha\rho_c e_c \Delta t E_y \delta \quad (8)$$

Where \square (reciprocal of the time period) is the frequency of the applied voltage, α is a factor to

account for the collision efficiency, ρ_c is the electron number density, e_c is the charge of the electron, Δt is plasma discharge time, much smaller than the time scale of the fluid and E is the electric field strength. The Dirac delta function means that the body force acts only in the regions in which the plasma is present:

$$\begin{cases} \delta = 1 & \text{for } E < E_{cr} \\ \delta = 0 & \text{for } E \geq E_{cr} \end{cases} \quad (9)$$

The E_{cr} in this case is the breakdown electric field strength, E_b .

To solve these equations, plasma-induced body force (\mathbf{b}) is added as a source term to the momentum equation in FSI solver. For the pressure equation the geometric algebraic multi grid (GAMG) solver and for velocity equations preconditioned bi-conjugate gradient (PBiCG) solver are used.

2.2 Mesh Motion Solver

The Fluid mesh motion is often considered as a third field besides the two-fields of fluid-structure problem. In general, the mesh motion is calculated using different ways such as: 1) using a spring analogy where all point-to-point mesh connections are replaced with springs, 2) casting the mesh as a pseudo solid, 3) modeling the mesh motion with the Laplace operator as described by Jasak and Tukovic (2006). Jasak and Tukovic have implemented their Laplacian method for moving mesh in OpenFOAM. This method involves the decomposition of OpenFOAM's arbitrary polyhedral mesh into tetrahedral element which moves according to the Laplace equation:

$$\nabla \cdot (\gamma \nabla \mathbf{v}^m) = 0 \quad (10)$$

Where γ is the diffusion coefficient that can be constant or variable throughout the fluid domain.

2.3 Structure Solver

Mass and linear momentum conservation equations for the motion of an isothermal continuum are as follows (Jasak and Tukovic (2007)):

$$\frac{d}{dt} \int_V \rho_s dV + \oint_S \mathbf{n} \cdot \rho_s (\mathbf{v} - \mathbf{v}_s) dS = 0 \quad (11)$$

$$\frac{d}{dt} \int_V \rho_s \mathbf{v} dV + \oint_S \mathbf{n} \cdot \rho_s (\mathbf{v} - \mathbf{v}_s) \mathbf{v} dS =$$

$$\oint_S \mathbf{n} \cdot \boldsymbol{\sigma} dS + \int_V \rho_s \mathbf{f}_b dV \quad (12)$$

where ρ_s is the continuum density, \mathbf{n} is the outward pointing unit normal to the surface S , \mathbf{v} is the velocity of the continuum, \mathbf{v}_s is the velocity of the surface S , $\boldsymbol{\sigma}$ is the Cauchy stress tensor and \mathbf{f}_b is the resulting body force. More information about the Lagrangian methodology applied to these equations

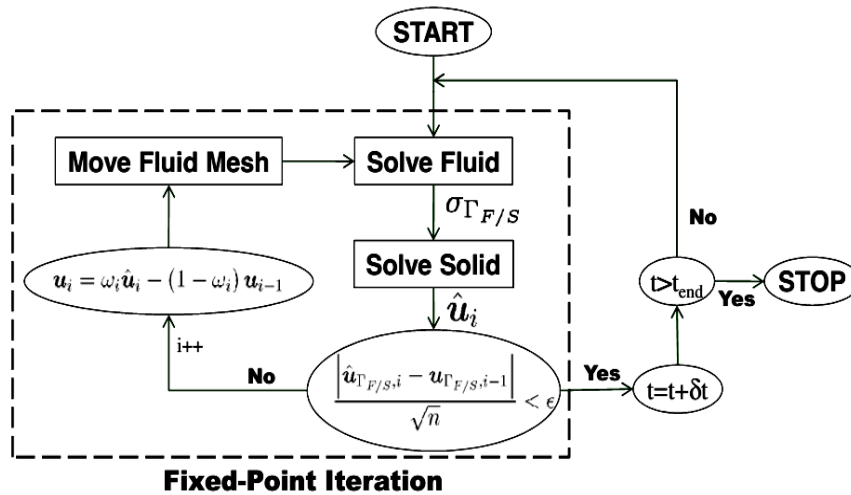


Fig. 2. Partitioned approach to FSI showing a fixed-point iteration with underrelaxation for tightly coupled solutions by Campbell (2010).

and finite volume discretization can be found in Jasak and Tukovic (2007).

2.4 FSI Solver

Partitioned procedure is utilized as the FSI solver for this work. This method uses a staggered solution method in which each domain is solved and the results are transferred between the solvers. The most basic method used by Piperno *et al.* (2001) is the CSS method, which first includes forecast of solid motion ($u^{n+1,p}$), then solving to obtain the stresses acting on the solid (σ_s^{n+1}), and finally solving the solid domain (u^{n+1}). The CSS method does not guarantee convergence of the FSI problem because there is no survey that matches predicted solid displacements by the calculated displacement at the end of the step. Thus this algorithm provides a weak coupling. Coupling strength depends on the degree of convergence of the fluid and solid domains at any time during the solution. Weak coupling consists of explicit time integration, even though integration of other factors may be implicit. Similarly, a strong coupling consists of implicit integration.

Weak coupling algorithm will be converted to a tight coupling with an iteration corrector step at each solution step (Matthies and Steindorf (2002)). This correction ensures the calculated solid displacement in accordance with predicted displacement in the CSS algorithm in each solution step. The most popular method of strong coupling is the fixed point iteration. However, the convergence of fixed point iteration is slow and the Aitken extrapolation is used in the present work to accelerate the convergence (Heil (2004)). Fig. (2) shows the details of the fixed point loop.

Information about the fluid stress must be transferred from the flow solver to the solid solver and information about the displacement must be

transferred from the solid solver to the flow solver. In terms of equations, following conditions are required for compatibility and no-slip condition:

$$v^m = \frac{du}{dt} \quad \text{On the interface} \quad (13)$$

$$\sigma^S \cdot n = \sigma^F \cdot n$$

Where n is the unit normal on the interface and the superscripts on σ denotes the stress for either the fluid or solid domain.

3. THE MESH AND BOUNDARY CONDITIONS

Airfoil geometry is shown in Fig. (3). A structured C-type grid is created for fluid domain with the Pointwise software. Grid and Boundary conditions for the fluid domain are shown in Fig. (4). Mesh is denser near the surface of the airfoil. No-slip boundary condition is used at the airfoil surface. Inlet and upper and lower boundaries are located at 12.5C from the airfoil surface and the output boundary is located at 21C. Slip boundary condition is used for the upper and lower boundaries. For the inlet boundary, velocity is calculated based on the desired Reynolds number and pressure gradient is zero. In the outlet boundary, pressure is equal to the free stream pressure and the velocity gradient is zero.



Fig. 3. NACA0012 airfoil Geometry.

Grid for solid domain is unstructured. Since current problem is two-dimensional, to impose pitching and flapping motions to the FSI case, two constraints are created, one on the center of mass and other on the quarter chord and two sinusoidal motions with different amplitudes are applied to them. Grid for the solid domain is shown in Fig. (5).

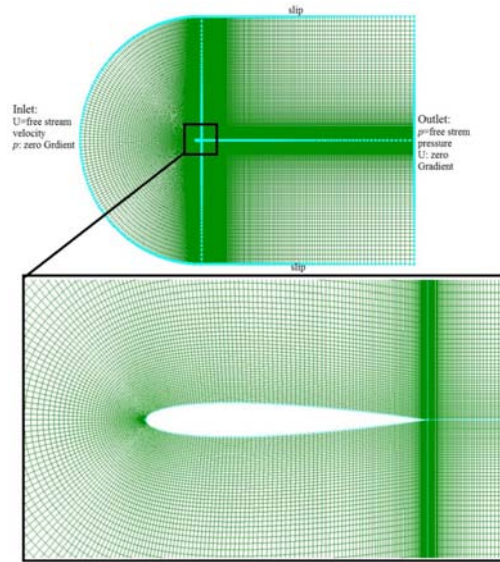


Fig. 4. Computational domain and boundary conditions of the fluid region.

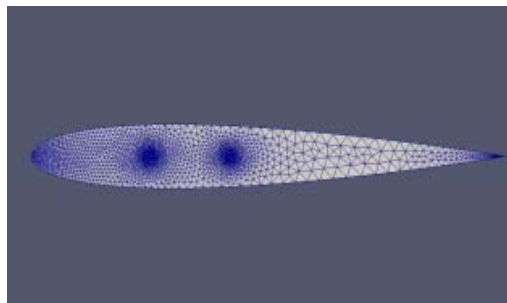


Fig. 5. Computational domain for solid region.

4. OSCILLATING AIRFOIL VALIDATION

In order to validate, pitching and plunging airfoil simulation results are compared with the results of Liang and Ou (2011).

For the pitching motion, amplitude of $A = 2^\circ$ and reduced frequency of $k = 6.68$ are used. As shown in Fig. (6), the maximum and minimum coefficients of lift using SD are equal to 2.95 and -2.98 respectively, while the corresponding values using OpenFOAM (present work) are 2.98564 and -2.97989. Maximum and minimum drag coefficients using SD are 0.0656 and -0.0412 and in our simulations they become 0.064896 and -0.04572, which are in good agreement with each other. Hence, the average error for the lift and drag coefficients respectively are 0.59% and 4.94%.

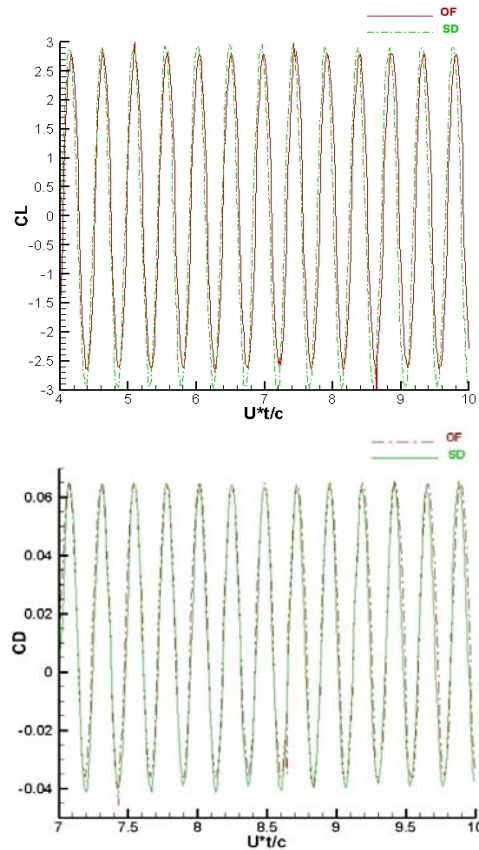


Fig. 6. Comparison between the present work, finite volume method in OpenFOAM (OF), and Spectral Difference method (SD) to calculate Lift and Drag coefficients.

For plunging airfoil, the amplitude and frequency of oscillation is considered exactly similar to section 4.2 of Liang and Ou (2011). As shown in Fig. (7), the maximum and minimum coefficients of lift using Spectral difference were respectively equal to 4.77 and -4.78, and using OpenFOAM simulation they became equal to 4.74268 and -4.73022. So there is no significant difference between the Spectral difference and OpenFOAM. Maximum and minimum drag coefficients are equal to 0.1 and -0.181 using Spectral difference and in our simulations they obtained as 0.1 and -0.18461 that have good agreement with previous data.

5. FSI SOLVER VALIDATION

In this section we discuss the FSI solver validation for the benchmark problem of flexible plate attached to a cylindrical rigid body, and subjected to an incompressible laminar flow. Structured grid of flow field and solid domain are shown in Fig. (8). Dimensions, geometry and boundary conditions are exactly the same as the Hron and Turek (2006) benchmark. Comparison is established for the case with density ratio 1, which leads to a strong coupling. As shown in Figs. (9) and (10), the results of OpenFOAM have a good agreement with the numerical results of Hron and Turek (2006).

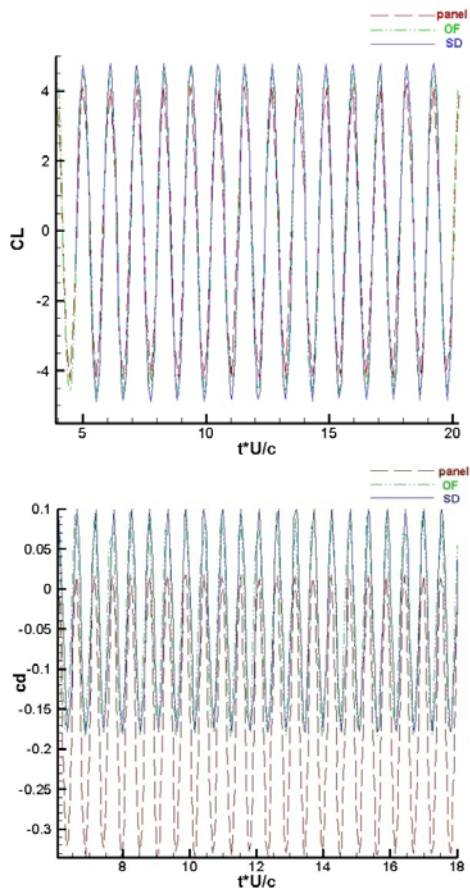


Fig. 7. Comparison between the present work, finite volume method in OpenFOAM (OF), and two other methods, Spectral Difference method (SD) and the Panel method to calculate Lift and Drag coefficients.

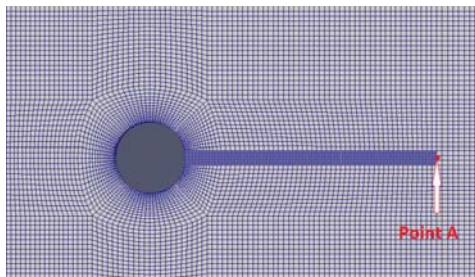


Fig. 8. Fluid and solid computational domain.

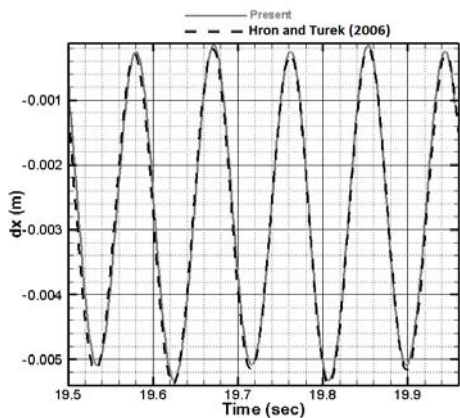


Fig. 9. Horizontal displacement of point A.

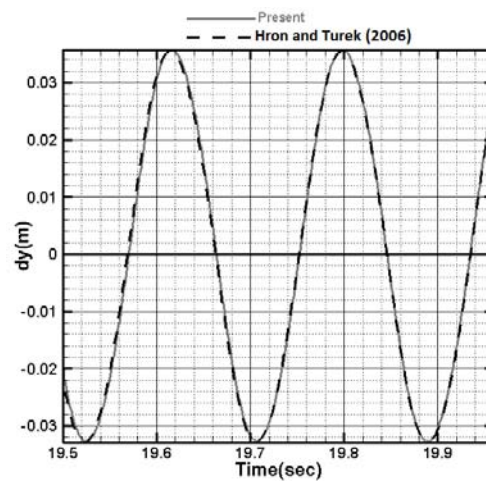


Fig. 10. Vertical displacement of point A.

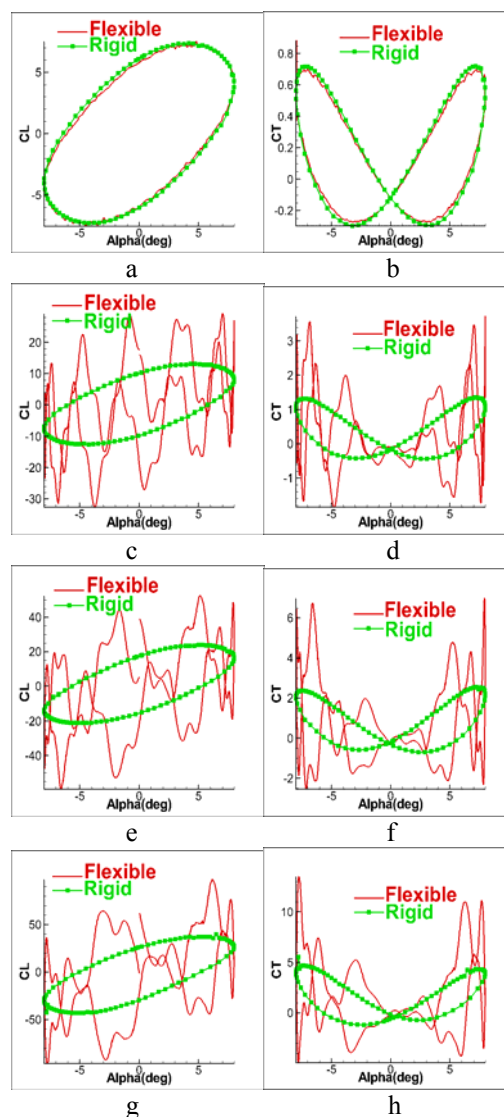
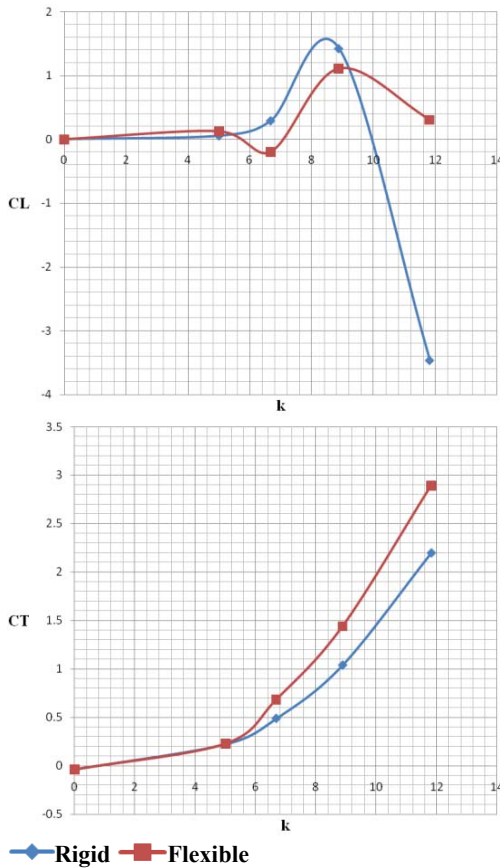


Fig. 11. Comparison of rigid and flexible airfoil characteristics for pitching amplitude $A=8^\circ$ and reduced frequencies $k=5.01, 6.68, 8.88, 11.82$, respectively; lift coefficients (a, c, e, g) and thrust coefficients (b, d, f, h).

6. RESULTS AND DISCUSSIONS

In this section numerical study of two dimensional laminar incompressible flow around a flexible oscillating NACA0012 airfoil will be presented. The results of both rigid and flexible airfoil will first be compared without considering the plasma actuation. Then the results of plasma actuated rigid and flexible airfoils will be compared. Airfoils are assumed to be made of PDMS material with

$$E = 2.75 \times 10^6 \text{ Pa}, \rho = 1320 \frac{\text{kg}}{\text{m}^3}, \nu = 0.35$$



◆ Rigid ■ Flexible
Fig. 12. Comparison of lift and thrust coefficients versus frequency of pitching motion for both rigid and flexible airfoils.

6.1 Comparison of Non-Actuated Airfoils

6.1.1 Pitching Motion

The lift and thrust coefficients of rigid and flexible airfoil are compared in Fig. (11) for amplitude of $A=8^\circ$ and four reduced frequencies of $k=5.01, 6.68, 8.88$ and 11.82 , respectively. As is clear from the figure, curves of the lift and thrust at lower frequencies are coincident and with increasing the frequency and the flexibility effect due to the effects of flow-induced vibrations, the curves of the flexible airfoil fluctuate around curves of the rigid airfoil.

As seen in Fig. (12), up to the frequency value of 5.01 , lift curves of both rigid and flexible airfoil are close together. Beyond this frequency two graphs

have the similar trend, but the lift of flexible airfoil decreases with the frequency at a lower slop. However the thrust increases with increasing the frequency and the value of thrust is higher for the flexible airfoil at higher frequencies. Therefore, it is found that at higher frequencies, it can be expected that both of the lift and thrust characteristics be improved.

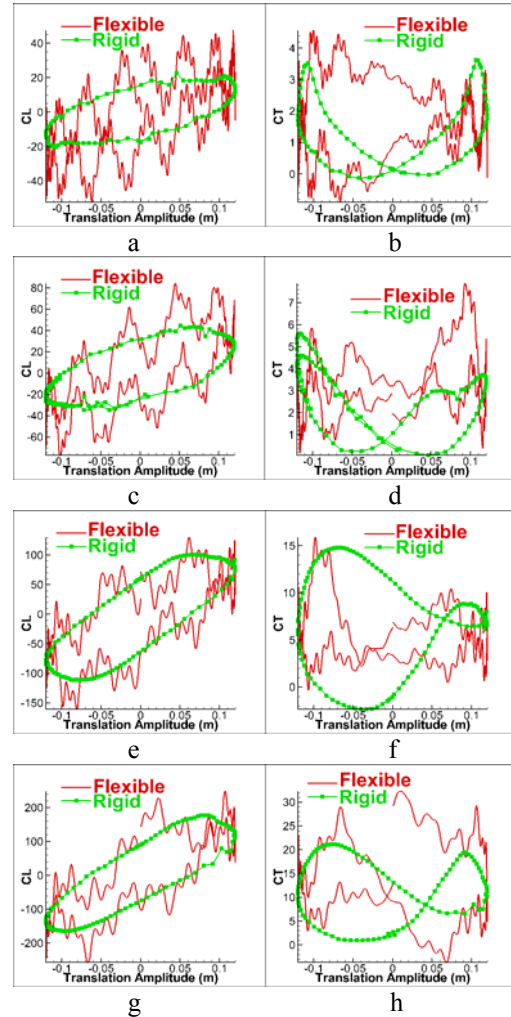


Fig. 13. Comparison of rigid and flexible airfoil characteristics for pitching amplitude $A=4^\circ$ and plunging amplitude $h=0.12c$ and reduced frequencies $k=5.01, 6.68, 8.88, 11.82$, respectively; lift coefficients (a, c, e, g) and thrust coefficients (b, d, f, h).

6.1.2 Flapping Motion

Figure (13) shows the hysteresis loops of the lift and thrust coefficients for the pitching amplitude of $A=4^\circ$, plunging amplitude of $h=0.12c$ and reduced frequencies of $k=5.01, 6.68, 8.88$ and 11.82 . As it is evident from the thrust curves, airfoil flexibility causes increasing thrust compared to the rigid case.

As seen in Fig. (14), in this type of motion, at reduced frequencies less than 8 , lift of the flexible airfoil is less than the rigid one but for frequencies greater than 8 , this trend is reversed and flexibility

improves the lift. While in pitching motion, beyond the frequency of 10.4, flexibility can improve the lift. Thrust is always increased with increasing the frequency and this increase is more severe for flexible airfoil. It can therefore be concluded that in the flapping motion, flexibility is more advantageous than the other motion type.

6.2 Comparison of Two Airfoils in Trailing Edge Plasma Actuation

6.2.1 Pitching Motion

Figure (15) shows the lift and thrust curves for plasma applied to the trailing edge of the pitching motion with the amplitude of $A=4^\circ$ and the reduced frequencies of $k=5.01, 6.68, 8.88$ and 11.82 . Fig. (16) compares the rigid and flexible airfoils at this motion type. As it is clear, the lift of the flexible airfoil is higher than the rigid airfoil and of course with increasing the frequency, the lift of both airfoils decreases. The Thrust curve of the flexible airfoil is lower than the rigid one, up to the frequency of 8.88 and then slowly increases. In fact, proximity of plot of thrust in both cases can be attributed to the small frequency and amplitude considered for this type of motion. Different diagrams may be obtained for higher frequencies and amplitudes. However, according to the trend of the graphs, it is expected that the flexibility improve both coefficients of lift and thrust.

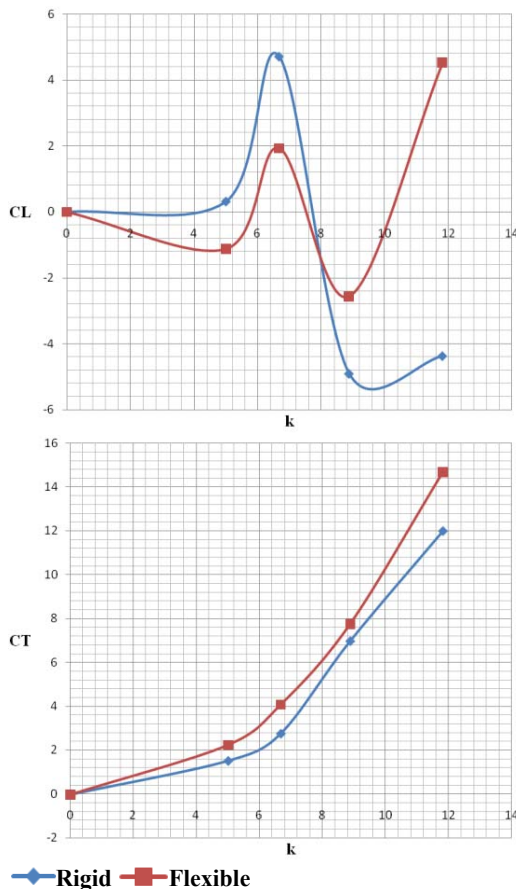


Fig. 14. Comparison of lift and thrust coefficients versus frequency of flapping motion for both rigid and flexible airfoils.

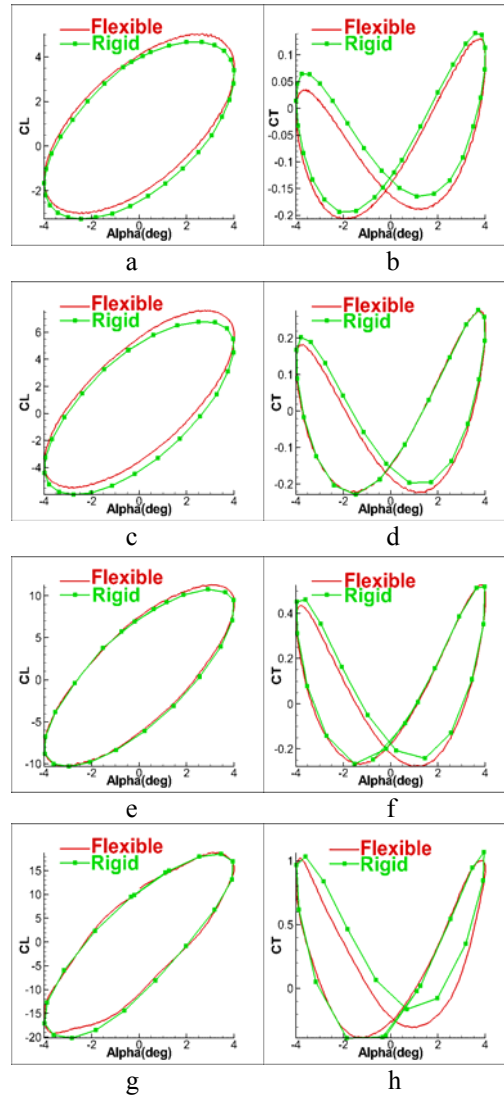


Fig. 15. Comparison of rigid and flexible airfoil characteristics for trailing plasma for pitching amplitude $A=4^\circ$ and reduced frequencies $k=5.01, 6.68, 8.88, 11.82$, respectively; lift coefficients (a, c, e, g) and thrust coefficients (b, d, f, h).

6.2.2 Flapping Motion

Figure (17) shows hysteresis loops of lift and thrust coefficients for pitching oscillation amplitude of $A=4^\circ$, plunging amplitude of $h=0.12c$ and reduced frequencies of $k = 5.01, 6.68, 8.88$ and 11.82 . In Fig. (18), it is shown that the lift curve of the flexible airfoil between the frequencies of 2 and 8 is less than the rigid one and for the frequencies higher than 8 or lower than 2, the frequency causes the lift of flexible airfoil to increase rather than the rigid one. But flexibility has a completely negative effect on the thrust, while rigidity has a positive effect in the case without plasma actuation (compare thrust curves in Figs. (14) and (18)). The reason may lie in several physical phenomena. The number and size of the vortices in flexible airfoil due to the flow induced body vibrations are much more than the rigid one. Moreover flapping

oscillation causes the vortex-body interaction that depends on the rotational forces and timing, it can result an increase or even decrease in the lift based on the rotational phase. The sum of these vortices and airfoil tail-induced vortices will affect the flow characteristics.

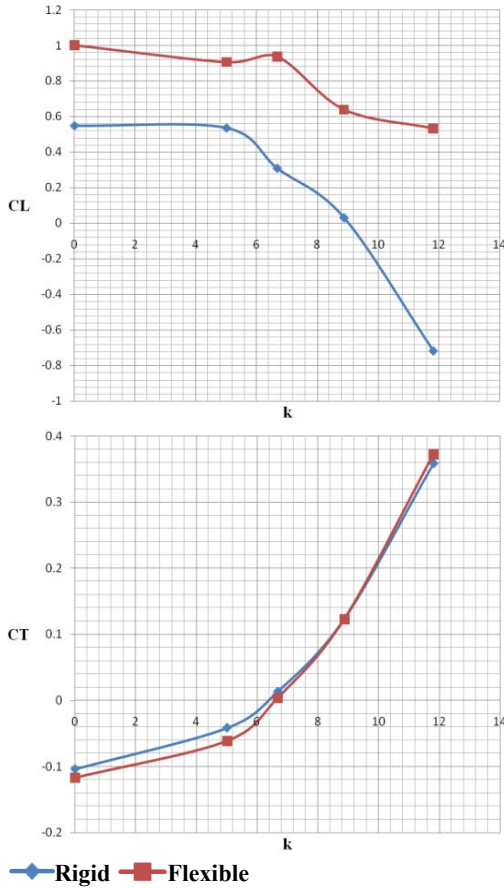


Fig. 16. Comparison of lift and thrust coefficients versus reduced frequency of pitching motion for both rigid and flexible airfoils at trailing edge plasma.

7. CONCLUSION

In this paper, the effect of flexibility of a 2D airfoil is investigated considering the solid-fluid interaction. To validate the developed OpenFOAM solver, the obtained results were compared to the benchmark simulation of incompressible laminar flow around a flexible plate attached to a cylindrical rigid body, and a very good agreement was detected. Then the effects of airfoil flexibility and flow induced vibrations on two oscillating motions and also the effect of reduced frequency on aerodynamic coefficients were investigated and compared with rigid airfoil. It was observed that in most of the cases the flexibility in both types of motions will improve the thrust and also the improvement will increase at higher frequencies. Unlike the thrust, a significant lift improvement may be achievable only at higher frequencies. It was also found that the effect of flexibility on flapping motion is more pronounced than pitching

motion.

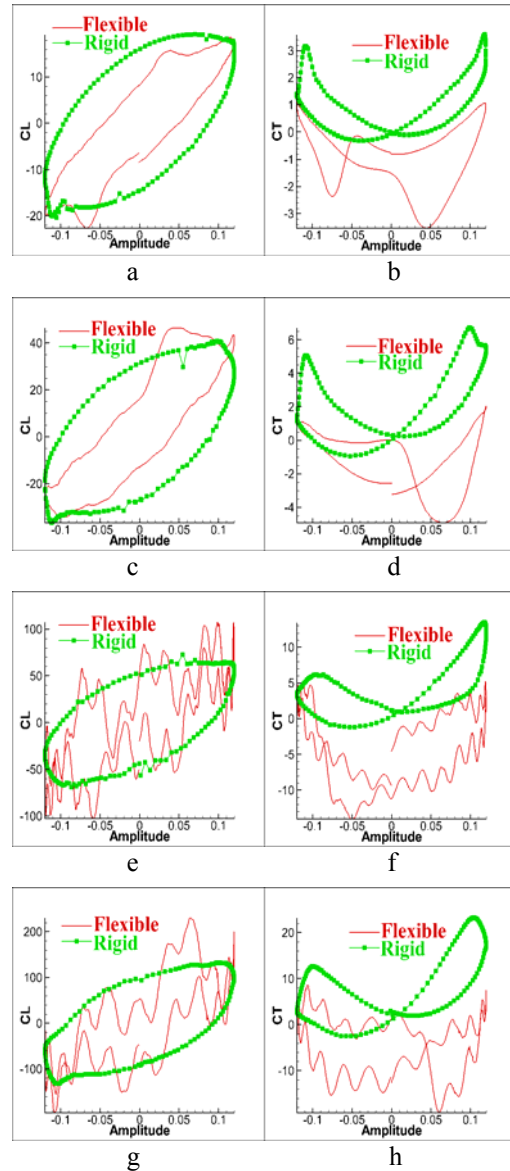


Fig. 17. Comparison of rigid and flexible airfoil characteristics for trailing edge plasma for pitching amplitude $A=4^\circ$ and plunging amplitude $h=0.12c$ and reduced frequencies $k=5.01, 6.68, 8.88, 11.82$, respectively; lift coefficients (a, c, e, g) and thrust coefficients (b, d, f, h).

By comparing the results of both rigid and flexible non-actuated airfoils, it can be concluded that:

- In pitching motion, Lift and thrust at lower frequencies are coincident and with increasing the frequency, lift of flexible airfoil decreases with a less slop. The thrust coefficient increases with an increment in frequency and the value of thrust coefficient is higher for the flexible airfoil.
- In flapping motion, at frequencies between 2 and 8, lift of the flexible airfoil is less than the rigid one but for frequencies greater than 8 or less than 2, this trend is reversed and flexibility

improves the lift. However, at higher frequencies, only for frequency values beyond 10.4 of flexible airfoil, “positive” lift coefficients occur. In this type of motion, the thrust is always increased with increasing frequency and flexibility.

By comparison of plasma actuated airfoils in both rigid and flexible cases, the following results are achieved:

- In pitching motion, lift of the flexible airfoil is greater than the rigid one and with increasing the frequency the lift of both airfoils decreases. Thrust of flexible case is lower than the rigid one up to a frequency value of 8.88 beyond which the magnitude of flexible case surpasses slightly.
- In flapping motion, lift of the flexible case at frequencies between 2 and 8 is less than the rigid one, beyond this area, lift of the flexible airfoil is placed at higher position than the rigid airfoil. Also, flexibility has a negative effect on thrust, unlike the case without plasma actuation.

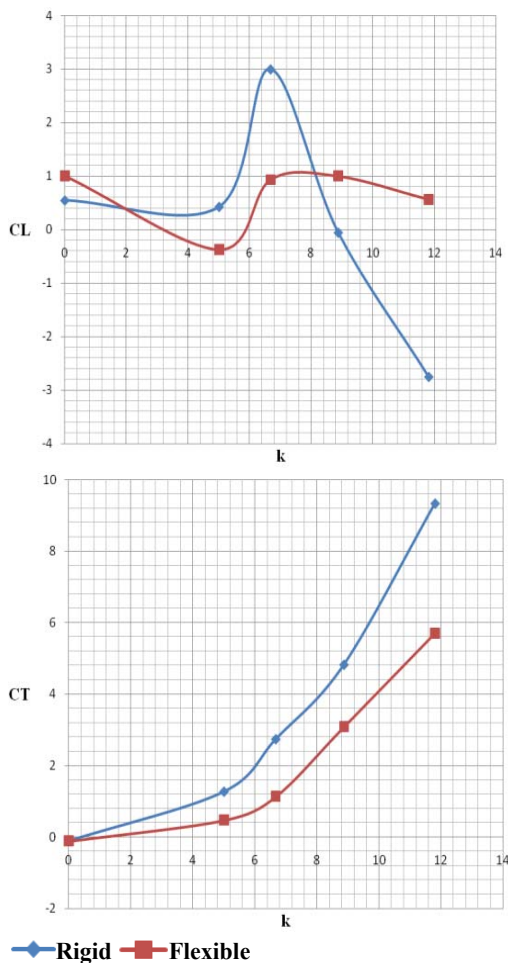


Fig. 18. Comparison of lift and thrust coefficients versus reduced frequency of flapping motion for both rigid and flexible airfoils at trailing edge plasma.

REFERENCES

Abdollahzadeh, M., J. Páscoa and P. Oliveira (2012). Numerical modeling of boundary layer control using dielectric barrier discharge. *In MEFTE IV Conferencia Nacional em Mecanica de Fluidos, Termodinamica e Energia* 63.

Campbell, R. L. (2010). *Fluid–structure interaction and inverse design simulations for flexible turbomachinery*. Submitted in Partial Fulfillment of the Requirements for the Degree of Doctor of Philosophy, The Pennsylvania State University.

Corke, T. C., M. L. Post and D. M. Orlov (2007). SDBD Plasma Enhanced Aerodynamics: Concepts, Optimization and Applications, *Progress in Aerospace Sciences* 43(7–8), 193–217.

Ducoin, A., J. A. Astol and J. F. Sigrist (2012). An experimental analysis of fluid structure interaction on a flexible hydrofoil in various flow regimes including cavitating flow. *European Journal of Mechanics - B/Fluids* 36, 63-74.

Heil, M. (2004). An efficient solver for the fully coupled solution of large-displacement fluid–structure interaction problems. *Computer Methods in Applied Mechanics and Engineering* 193(1-2), 1–23.

Jasak, H. and Z. Tuković (2006). Automatic mesh motion for the unstructured finite volume method. *Transactions of FAMENA* 30(2), 1–20.

Kamakoti, R. and W. Shyy (2004). Fluid–structure interaction for aeroelastic applications. *Progress in Aerospace Sciences* 40(8), 535–558.

Kim, D. H. and J. W. Chang (2014). Low-Reynolds-number effect on the aerodynamic characteristics of a pitching NACA0012 airfoil. *Aerospace Science and Technology* 32, 162–168.

Lapointe, S. and G. Dumas (2012). Numerical Simulations of Self-Sustained Pitch-Heave Oscillations of a NACA 0012 Airfoil. *Presented at: 20th Annual Conference of the CFD Society of Canada, Canmore, Canada.*

Lee, J. and S. Lee (2012). Fluid–structure interaction analysis on a flexible plate normal to a free stream at low Reynolds numbers. *Journal of Fluids and Structures* 29, 18–34.

Lee, J. and S. Lee (2013). Fluid–structure interaction for the propulsive velocity of a flapping flexible plate at low Reynolds number. *Computers and Fluids* 71, 348–374.

Liang, C. and K. Ou (2011). High-order accurate simulations of unsteady flow past plunging and pitching airfoils. *Journal of Computers and Fluids* 40(1), 236–248.

- Matthies, H. and J. Steindorf (2002). Partitioned but strongly coupled iteration schemes for nonlinear fluid–structure interaction. *Computers and Structures* 80(27-30), 1991–1999.
- Mukherjee, S. and S. Roy (2012). Enhancement of Lift and Drag Characteristics of an Oscillating Airfoil in Deep Dynamic Stall Using Plasma Actuation. *Aerospace Sciences Meetings. 50th AIAA aerospace sciences meeting including the new horizons forum and aerospace exposition*.
- Olivier, M., G. Dumas and J. F. Morissette (2009). A Fluid-Structure Interaction Solver For Nano Air Vehicle Flapping Wings. *19th AIAA Computational Fluid Dynamics*, 2009-3676, San Antonio, Texas.
- Piperno, S. and C. Farhat (2001). Partitioned procedures for the transient solution of coupled aeroelastic problems—part II: energy transfer analysis and three-dimensional applications. *Computer Methods in Applied Mechanics and Engineering* 190(24-25), 3147–3170.
- Shyy, W., B. Jayaraman and A. Andersson (2002). Modeling of Glow Discharge Induced Fluid Dynamics. *Journal of Applied Physics* 92(11), 6434–6443.
- Tang, J., S. Chimakurthi, R. Palacios, E. S. Carlos and W. Shyy (2008). Computational Fluid-Structure Interaction of a Deformable Flapping Wing for Micro Air Vehicle Applications. *46th AIAA Aerospace Sciences Meeting and Exhibit*, Reno, Nevada.
- Tezduyar, T. E., S. Sathe, J. Pausewang, M. Schwaab, J. Christopher and J. Crabtree (2008). Interface projection techniques for fluid-structure interaction modeling with moving-mesh methods. *Computational Mechanics* 43(1), 39–49.
- Tuković, Ž. and H. Jasak (2007). Updated Lagrangian finite volume solver for large deformation dynamic response of elastic body. *Academic Journal* 31(1), 55.
- Turek, S. and J. Hron (2006). Proposal for numerical benchmarking of fluid-structure interaction between an elastic object and laminar incompressible flow. *Lecture Notes in Computational Science and Engineering* 53, 371-385.
- Unger, R., M. C. Haupt, and P. Horst (2008). Numerical simulation of an oscillating and flexible airfoil for flapping wing propulsion with fluid-structure interaction. In *26th International Congress of the Aeronautical Sciences*, 321, Anchorage, Alaska, USA.
- Unger, R., M. C. Haupt, P. Horst and R. Radespiel (2012). Fluid–structure analysis of a flexible flapping airfoil at low Reynolds number flow. *Journal of Fluids and Structures*, 28, 72–88.
- Veilleux, J. C. and G. Dumas (2013). May 6th to 9th), Numerical Simulations of Experimentally Observed High-Amplitudes, Self-Sustained Pitch-Heave Oscillations of a NACA 0012 Airfoil. Presented at: *21th Annual Conference of the CFD Society of Canada*, Sherbrooke, Canada.
- Walker, S. and T. Segawa (2012). Mitigation of flow separation using DBD plasma actuators on airfoils: A tool for more efficient wind turbine operation. *Renewable Energy* 42, 105-110.
- Zhang, P. F., A. B. Liu and J. J. Wang (2009). Aerodynamic modification of a NACA 0012 airfoil by trailing-edge plasma Gurney flap. *AIAA Journal* 47(10), 2467-2474.